JOURNAL OF MATERIALS SCIENCE 13 (1978) 323–328

The metallography of fracture in cast nickel aluminium bronze

E. A. CULPAN
AUWE, Portland, Dorset, UK

J. T. BARNBY
Department of Metallurgy and Materials, University of Aston, Birmingham, UK

In tube burst tests, and in slow bend tests, crack propagation in nickel aluminium bronze produces crack faces normal to the tension stress even though plastic deformation preceding fracture occurs under conditions of generalized plane stress. Shear lips are observed to be about 1.0 mm deep and, therefore, much less than the critical plane stress plastic zone radius which is around 40 to 50 mm in tube tests. Fractographic and metallurgical examinations reveal that the crack path is dictated by metallurgical structure and that the small shear lips and flatness of the crack faces arise from a cumulative mode of fracture dictated by structural features rather than as a result of constraint stresses.

1. Introduction

The fine structure of fracture surfaces arise from the operation of various microscopic mechanisms [1] of fracture dictated by the inhomogeneous structure of engineering alloys. In spite of this the macroscopic Mode I [2] fracture appearance generally conforms to expectations arising from engineering considerations of a homogeneous solid, metallurgical structures dictating only that some mechanism of dilatation by void growth occurs when plastic flow at the crack tip is constrained to take place under plane strain conditions. When these constraints do not exist such as in crack propagation in thin sheets or near the side surface of thick plates, the fracture is of the shear type. [3] Here fracture occurs along the plane of maximum shear stress giving the shear lips of a fracture surface as illustrated in Fig. 1.

The depth of the shear lips is normally approximately equal to the radius of the plane-stress plastic zone in which the microstructural mechanisms operate, indeed the effect of thickness on fracture toughness may be explained by supposing the material to have two different energy consumption rates in fracture, corresponding to generation of the slant and flat fracture surfaces. [4] In spite of this, the experiments described below produced shear lips which bore no relation to the critical plastic zone size, and also flat fracture surfaces were generated in specimens of a thickness which would normally be expected to give rise solely to slant fractures.

In macroscopic terms flat fractures occur when constraint stresses produce a hydrostatic component to the stress field such that the normal stress operates fracture mechanisms at a lower level than is required for yield on the Von Mises or the Tresca condition. [5] Furthermore, the crack path is macroscopically dictated by geometric features giving rise to a maximum energy release rate path. [6] In contrast, the flatness of fractures described here arises from special metallurgical features of the case structure, which in principle could also dictate macroscopic cracking directions in the same way as they dictate microscopic directions.

An appreciation of the above factors which emerge from metallographic investigation indicates principles by which toughness of cast metals may be improved by control of metallurgical structures.

2. Experimental materials and methods

The BS 1400. AB2 nickel aluminium bronzes tested were within the compositional limits

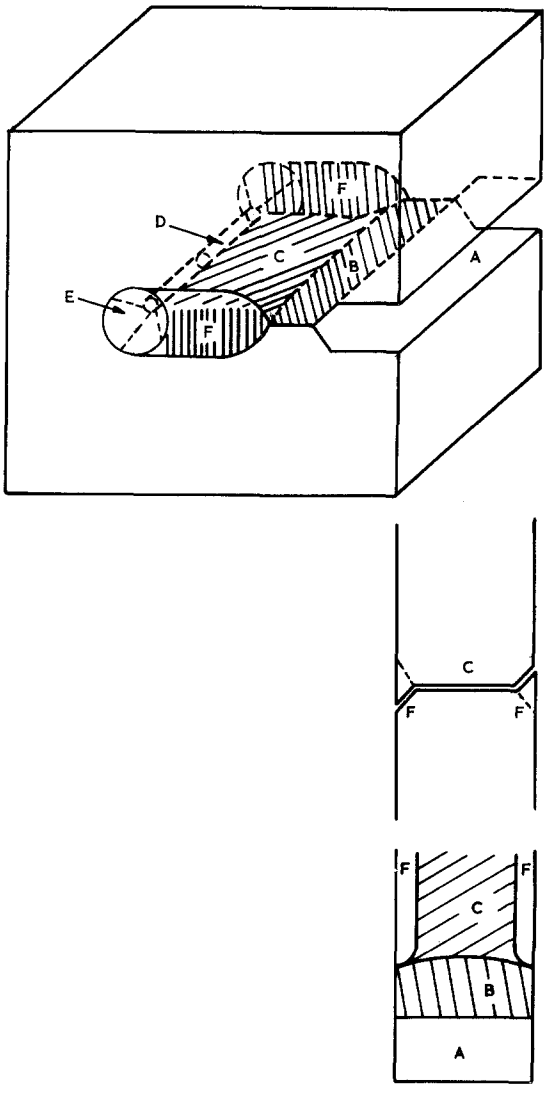

Figure 1 Diagrametic representation of the relationship between shear lips and plastic zone size; notch (A); fatigue crack (B); flat plane strain (C); plane strain plastic zone (D); plane stress plastic zone (E); shear lips (F).

listed in Table I. Bend specimens were nominally 160 mm long, 10 mm thick, (B) and 30 mm deep, (W). Notches were cut about 10 mm deep, giving a/w ratios of about 0.3, and tests carried out in three point bending using a machine crosshead speed of 0.505 mm min^{-1}. Toughnesses, K_c, for these specimens with spark machined notches or with pre-fatigue cracked notches were in the range 114 MN $m^{-3/2}$ to 134 MN $m^{-3/2}$, these figures being derived from J-integral type tests. [7]

Internal pressure tests were carried out on tubes with an internal diameter of 101.6 mm and a wall thickness of 9.5 mm, containing axial spark-machined slots. Toughness values from the tube bursts generally fell within the range 125 MN $m^{-3/2}$ to 175 MN $m^{-3/2}$, so that an average value of the K_c would be 150 MN $m^{-3/2}$ [8]. Scatter in the experiments is believed to arise mainly from variation of the properties of the individual cast tubes. However, all tubes and bend specimens were of high toughness.

TABLE I Composition (wt %)

Al	Fe	Ni	Mn	Cu
9.4–10.0	4.3–4.7	4.8–5.0	1.2–1.4	Balance

3. Results

3.1. Metallographic structures

Nickel aluminium bronze solidifies as the β phase. On further cooling the α phase grows at the β grain-boundaries and along crystallographic planes (Fig. 2) to form a "Widmanstatten" structure [9].

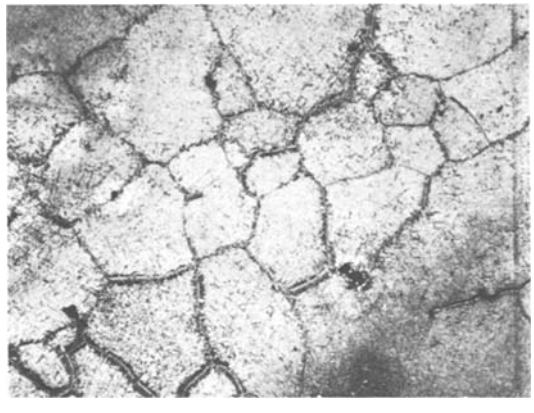

Figure 2 β grain size. (X14).

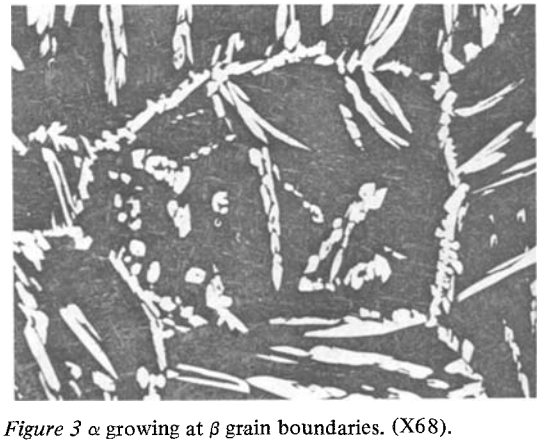

Figure 3 α growing at β grain boundaries. (X68).

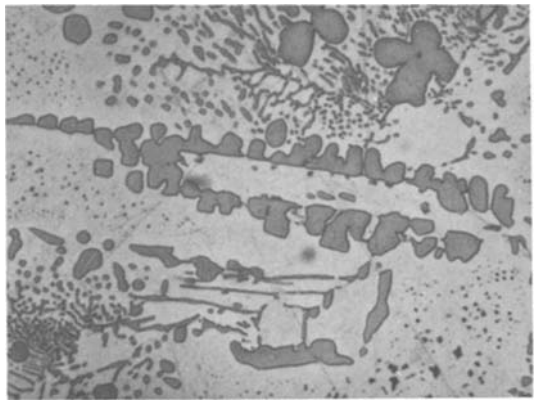

Figure 4 κ_1 precipitates in straight lines. (X1088).

An indication of the original β grain size is given in Fig. 3 which is taken from a sample of nickel aluminium bronze quenched from 1000° C into cold water. It can be seen that grain size of the β phase is approximately 0.5 mm.

At high temperatures the iron rich κ phase, similar to Fe_3Al [10] forms with a rosette morphology κ_I, typical of relatively rapid and long range diffusion conditions. The κ_I precipitates often occur in straight lines across α grains as shown in Fig. 4, which could indicate the presence of annealing twins acting as nucleation sites. At lower temperatures two further discontinuous forms of κ precipitation occur; [11] κ_{II} as a rounded discontinuous phase on a polished section, and κ_{III} with a lamellar or pearlitic distribution. The κ_{II} and κ_{III} can exist over a range of compositions based on NiAl/FeAl. Finally, the central regions of α reject a fine precipitate, κ_{IV}, which affects the yield strength, and thus supports the view that the solubility boundary in the α curves back towards low aluminium concentrations at lower temperatures, affording some capacity for precipitation hardening [11]. The morphology of these phases is illustrated in Fig. 5.

3.2. Fracture paths

Examination of polished and etched side surfaces close to the crack tips in burst tubes shows a strong correlation between the distribution of κ_I and the fracture path, as shown in Fig. 6. Regions ahead of the arrested crack tip show boundaries

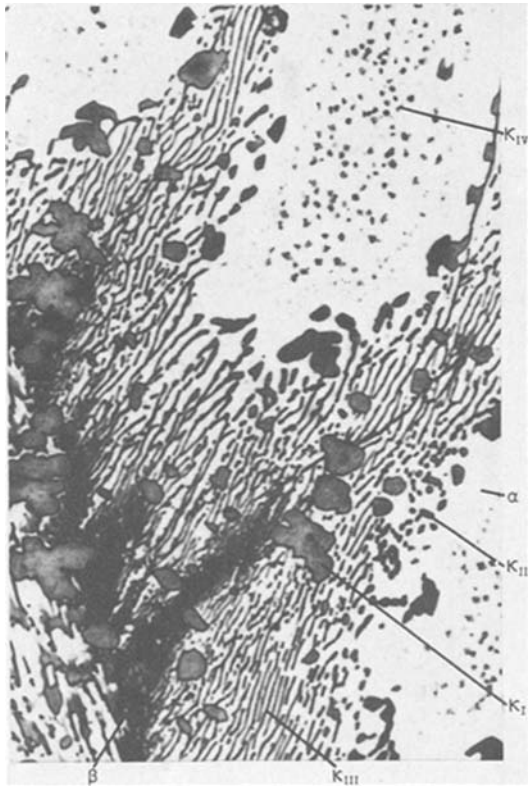

Figure 5 Microstructure of nickel aluminium bronze showing constituent phases. (X920).

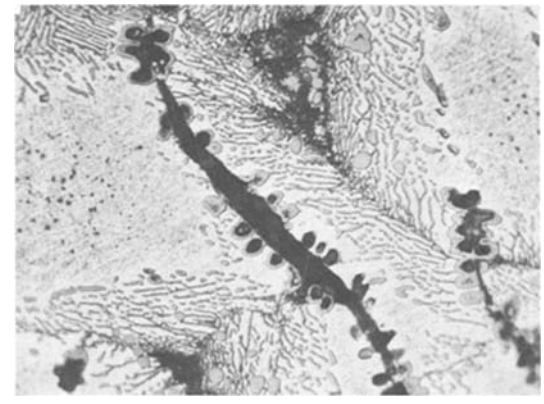

Figure 6 Tip of arrested crack. (X816).

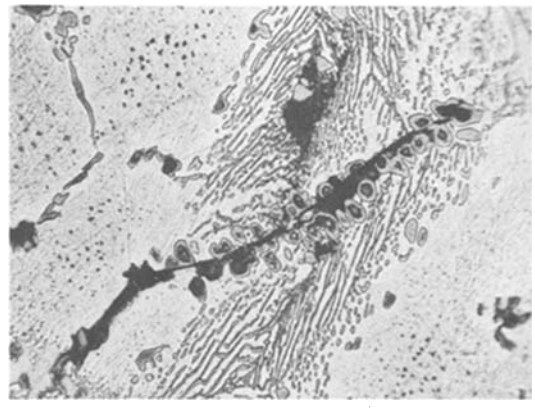

Figure 7 Ahead of arrested crack. (X816).

containing κ_I which have cracked open under the influence of strain within the plastic zone, as illustrated by Fig. 7. Often such preparatory damage emanates from micro-shrinkage pores, (Fig. 8) the cracking then following lines of κ_I phase. Broken halves of κ_I precipitates often decorate the crack edges as shown in Figs. 11 and 12.

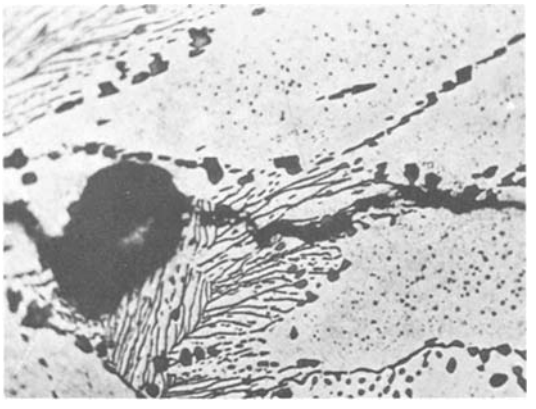

Figure 8 Preparatory damage adjacent to a microshrinkage pore. (X816).

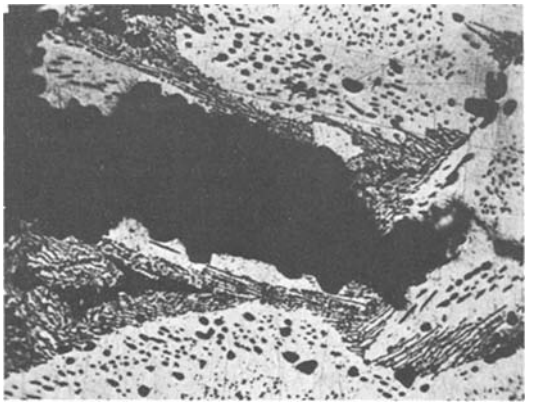

Figure 9 Crack edge showing broken precipitate particles along the fracture surface. (X816).

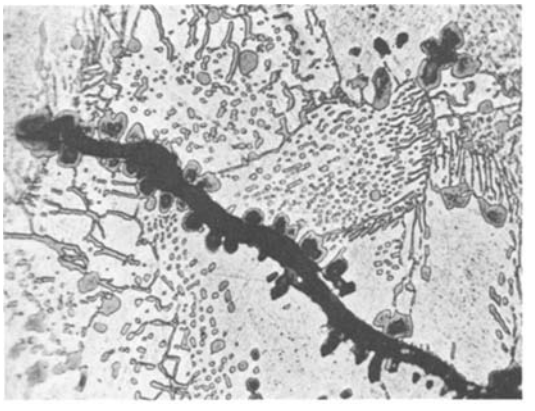

Figure 10 Broken precipitates along the edges of a crack tip. (X1200).

3.3. Fractography

At low magnification, fracture surfaces show dendritic patterns as in Fig. 11, whereas around magnifications of 816, as in Fig. 10, the fracture paths are often within the α grains. Of course, these are compatible aspects of the fracture path since the α grains outline the original β dendrite structure. Final fracture must occur across the α grains as well as between them. Such fracture surfaces show the highly ductile dimples as in the top region of Fig. 12, whereas the central region of Fig. 12 corresponds to a κ_I precipitate region, in an α boundary. The shear lips shown in Fig. 13 on the fracture surface of a bend specimen (which fractured after general yield) are only about 1 mm deep. Taking a toughness [8] of 150 MN m$^{-3/2}$ and a typical yield stress [8] of 280 MN m^{-2},

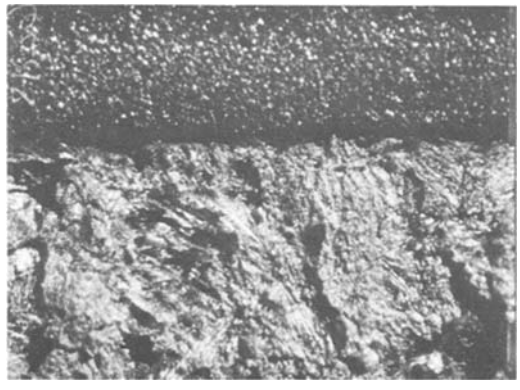

Figure 11 Fracture surface of a bend specimen showing a dendrite pattern. The upper region is the spark machined notch. (X20).

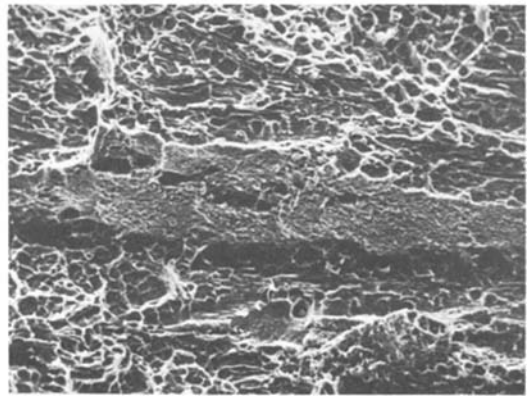

Figure 12 Fracture surface of a bend specimen. Scanning electromicrograph. (X340).

would indicate a plane stress plastic zone radius of 46 mm, given by:

$$r_y = \frac{1}{2\pi}\left(\frac{K_c}{\sigma_y}\right)^2 \quad (1)$$

In fact Fig. 11 shows shear lips which closely correspond to the size of the original β grains rather than to r_y.

One bend specimen taken from a thick cast section showed much larger shear lips (approximately 5 mm) than those normally found with this material. The fracture surface of this specimen is shown on the left hand side of Fig. 14 with a more usual fracture on the right. Fig. 15 shows the original β grain structure of the large shear lip material following a water quench from 1000° C. It can be seen that the β grain size of about 5 to 6 mm is also larger than that observed in previous specimens. This indicates a strong correlation between size of shear lips and the β grain structure even though the alloys have a very high toughness [7, 8].

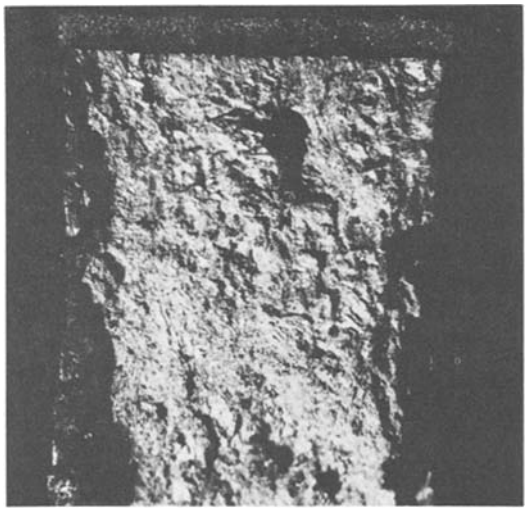

Figure 13 Fracture surface of a bend specimen showing shear lips of approximately 1 mm deep. (X5.4).

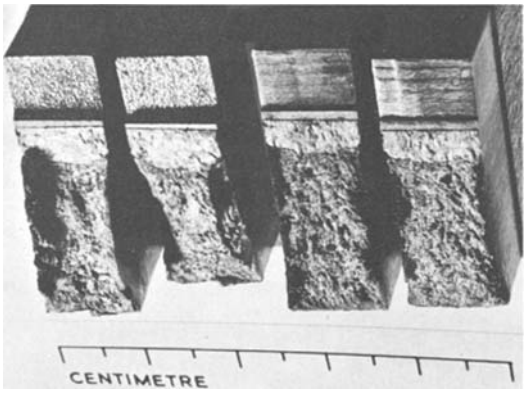

Figure 14 Fracture surfaces showing machined notch, spark machined regions, fatigue pre-cracked surface, fracture surfaces and shear lips.

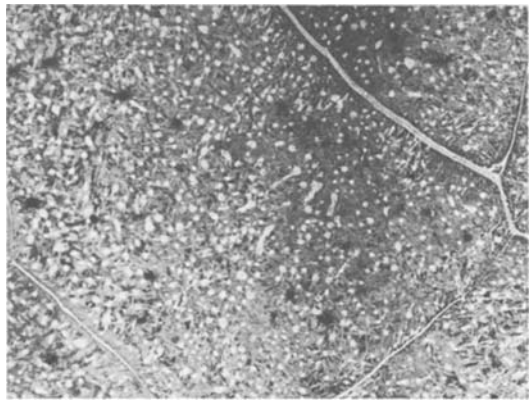

Figure 15 β grain size of large shear lip material shown in Fig. 14. (X14).

4. Discussion

The shear lips and flat fracture surface in Fig. 13 must arise from microstructural control and not from macroscopic control as is evidenced by their lack of correspondence with r_y. The structural damage shown in Figs. 7 and 8 exists up to 1 mm ahead of the actual check tip. Since the original β grain size is around 1.0 mm this damage exists within at least one dendrite size ahead of the crack tip. It is interesting that the preparatory damage is often initiated at micro shrinkage pores. This porosity is found where the last liquid metal solidified, i.e. at the original β grain boundaries. Moreoever, the damage is in planar areas as evidenced by Figs. 6, 7 and 11. There is, therefore, a considerable reduction in load carrying area within the near tip plastic zone. Both Cottrell [12] and Thomason [13] have linked the degree to which fracture is cumulative to the loss in sectional area within the near tip plastic zone, and the effect is more damaging if the loss of area is in the form of flat planar defects [12]. What is not predicted is that the fracture surface can become macroscopically flat as a result of this microstructural control. This occurs in the material studied here, together with shear lips which reveal that slant fracture occurs only through the final dendrite near the side surface, and even then only if the dendrite is unsuitably orientated for flat fracture.

Acknowledgements

The assistance of Mr L. J. Hussey and Mr M. S. Atherton during pressure testing and metallography is gratefully acknowledged. Any views expressed are those of the authors and do not necessarily represent those of the Procurement Executive, Ministry of Defence. This paper is published by permission of the Controller, HMSO, holder of Crown Copyright.

References

1. C. D. BEACHAM, "Fracture, An Advanced Treatise", Vol. I, edited by H. Liebowitz (Academic Press, New York, 1968) p. 243.
2. G. R. IRWIN, University of Illinois TAM Report No. 202.
3. W. F. BROWN and J. E. SRAWLEY, "Plane Strain Toughness Testing", STP 410 (ASTM, Philadelphia, 1966).
4. J. I. BLUHM, "Fracture Mechanics of Aircraft Structures", edited by H. Liebowitz (AGARD, Neuilly-sur-Seine, 1974) p. 74.
5. J. E. SRAWLEY and W. F. BROWN, "Fracture Toughness Testing and its Applications", STP 381 (ASTM, Philadelphia, 1965) p. 142.
6. G. C. SIH, "Mechanics of Fracture Vol. I: Methods of Analysis and Solutions of Crack Problems" (Noordhof, Leyden, Netherlands, 1973).
7. J. T. BARNBY, E. A. CULPAN, M. S. ATHERTON and D. M. RAE, *J. Mater. Sci.* **12** (1977) 1857.
8. J. T. BARNBY, E. A. CULPAN, A. E. MORRIS, L. J. HUSSEY, M. S. ATHERTON and D. M. RAE, *Int. J. Fracture* (to be published).
9. W. L. J. CROFTS, D. W. TOWNSEND and A. P. BATES, *British Foundryman* **57** (1964) 89.
10. P. J. MACKEN and A. A. SMITH, "The Aluminium Bronzes", Copper Development Association Publication No. 31, 1966.
11. E. A. CULPAN, G. ROSE and D. MOTH, Private communication.
12. A. H. COTTRELL, "Fracture", edited by C. J. Osborne (University of Melbourne, Melbourne, 1965) p. 1.
13. P. F. THOMSON, *Int. J. Fracture. Mech.* 7 (1971) 409.

Received 15 April and accepted 19 May 1977.